Showcasing research from Dr Xiao-Ying Yu at the Directorate of Earth and Biological Sciences, Pacific Northwest National Laboratory (PNNL), USA, in collaboration with her colleagues at PNNL.

Two coexisting liquid phases in switchable ionic liquids

For the first time, we have confirmed distinct non-ionic and ionic regions in the switchable ionic liquid at varied degrees of ionicity by *in situ* chemical imaging mass spectrometry, even when chemical stoichiometry would indicate a 100% ionic composition. The unique physical and thermodynamic properties of such liquids are linked to this biphasic liquid environment, which is vastly different from other conventional fluids or ionic liquids.

ROYAL SOCIETY
OF **CHEMISTRY**

rsc.li/pccp

Check for updates

Two coexisting liquid phases in switchable ionic liquids†

Juan Yao, [a] David B. Lao,‡[b] Xiao Sui, ‡[a] Yufan Zhou,‡[c] Satish K. Nune, [b]
Xiang Ma, [d] Tyler P. Troy, [e] Musa Ahmed, [e] Zihua Zhu, [c]
David J. Heldebrant [b] and Xiao-Ying Yu *[a]

Switchable ionic liquids (SWILs) derived from organic bases and alcohols are attractive due to their applications in gas capture, separations, and nanomaterial synthesis. However, their exact solvent structure still remains a mystery. We present the first chemical mapping of a SWIL solvent structure using *in situ* time-of-flight secondary ion mass spectrometry. *In situ* chemical mapping discovers two coexisting liquid phases and molecular structures vastly different from conventional ionic liquids. SWIL chemical speciation is found to be more complex than the known stoichiometry. Dimers and ionic clusters have been identified in SIMS spectra; and confirmed to be the chemical species differentiating from non-ionic liquids *via* spectral principal component analysis. Our unique *in situ* molecular imaging has advanced the understanding of SWIL chemistry and how this "heterogeneous" liquid structure may impact SWILs' physical and thermodynamic properties and associated applications.
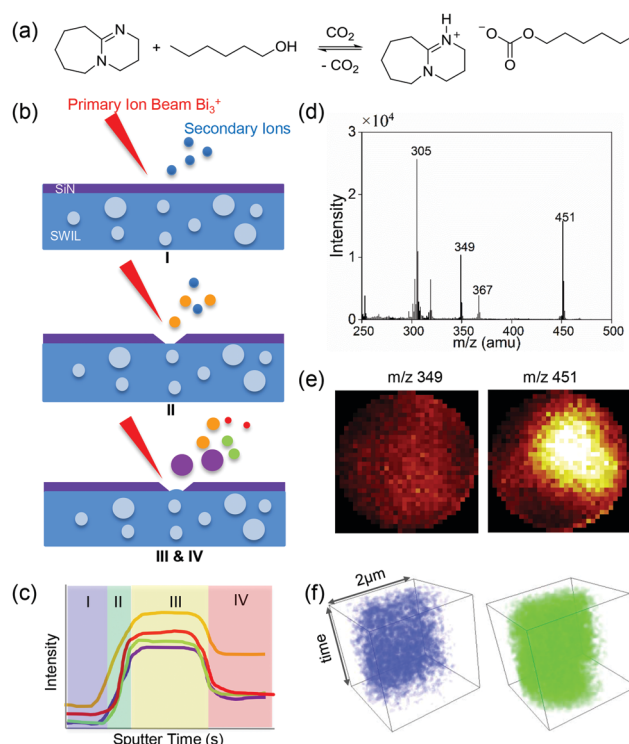
Fig. 1 Liquid ToF-SIMS analysis of SWILs. (a) The known DBU and 1-hexanol SWIL chemistry; (b) schematic of the SALVI and ToF-SIMS imaging and depth profiling process; (c) depth profiling time series of four species in different colour acquired from before SiN punch-through (region I, purple shade), during punch-through (region II, green), image acquisition (region III, yellow) and high mass resolution acquisition (region IV, salmon); (d) a *m/z* spectrum in the positive mode from region IV in (c); (e) re-constructed 2D images; and (f) 3D images of *m/z*+ 349 (blue) and 451 (green) from the 100% CO_2 loaded SWIL in the positive ion mode from region III in (c).

Switchable ionic liquids (SWILs) are solvent mixtures that change between non-ionic and ionic liquid forms by the addition or removal of an acidic gas.[1] They provide unique solvent properties necessary for green processes.[2] SWILs have many applications in CO_2 capture,[3,4] water-purification,[5] catalysis,[6,7] nanomaterial synthesis.[8,9] SWILs are comprised of CO_2-reactive species, most commonly an alcohol and an amine base.[1] One of the first SWILs consisted of 1-hexanol and 1,8-diazabicycloundec-7-ene (DBU).[1] It was predicted to react with CO_2 in a 1 : 1 molar ratio to form carboxylated ion pairs (Fig. 1a).[1] Removal of CO_2 can be

accomplished by heating, by sparging with nitrogen or argon, or vacuum, reverting the solvent to a non-ionic form.

The question that whether the structure of SWILs is similar to that of conventional ionic liquids (ILs) is intriguing. It is

[a] *Earth and Biological Sciences Directorate, Pacific Northwest National Laboratory, Richland, WA 99352, USA. E-mail: xiaoying.yu@pnnl.gov*

[b] *Energy and Environment Directorate, Pacific Northwest National Laboratory, Richland, WA 99352, USA*

[c] *W. R. Wiley Environmental Molecular Science Laboratory, Pacific Northwest National Laboratory, Richland, WA 99354, USA*

[d] *Dept. Chemistry, Idaho State University, Pocatello, ID 83209, USA*

[e] *Chemical Sciences Division, Lawrence Berkeley National Laboratory, Berkeley, CA, 94720, USA*

† Electronic supplementary information (ESI) available. See DOI: 10.1039/c7cp03754f

‡ Equal contribution.

This journal is © the Owner Societies 2017

Phys. Chem. Chem. Phys., 2017, **19**, 22627–22632 | 22627

hypothesized that SWILs are never truly 100% ionic, nor 100% non-ionic. Instead, they fluctuate between various states of mostly ionic or mostly non-ionic. Thus, it is unclear whether SWILs entail the same structural features that enable high performance in catalysis or synthesis of nanomaterials. ILs have been used to synthesize anisotropic nanostructures such as nanowires, partly because ILs contain an organized solvent structure that acts as a soft template inducing structural directionality during synthesis.[8,9] The organized solvent structure of ILs was postulated for metal ions to control the size and shape in nanoparticle formation.[10] If SWILs exert the same template effect, it is likely that they would share similar molecular structure to that of ILs. SWILs were proposed to have a similar structure to ILs at high degrees of ionicity (i.e., high CO_2 loading), resulting in a template effect.[8] However, it is unclear how the solvent would change its speciation and structure as a function of ionicity. The same is true concerning how such changes would impact the physical and thermodynamic properties of SWILs.

We recently demonstrated that SWILs exerted a template effect with high CO_2 loading, producing nanocrystalline green rust and 5 nm spherical magnetite particles.[8] A similar approach was used in the synthesis of gold nanoparticles with switchable carbamate ionic liquids.[11] The synthesis of nanoparticles using SWILs suggests that the structure of SWILs yield a somewhat ordered environment within a few nanometers, promoting nanoparticle nucleation and growth. However, such a liquid structure has yet to be determined.

After over a decade of research and hundreds of publications, the molecular structure of SWILs remains a mystery. It is unclear if ions would be uniformly distributed in solution like salt in water, or localized clusters of ions would aggregate like nano-sized micelles. Liauw proposed a heterogeneous solvent structure based on observations from Attenuated Total Reflectance (ATR) ultraviolet (UV) and infrared (IR) spectroscopy, showing disparate regions in carbonate concentration in contrary to the solvent stoichiometry.[12] Density Functional Theory (DFT) calculations were used to study the solvent structure of [1-((1,3-dimethyl-imidazolidin-2-ylidene)amino)propan-2-ol].[13] The simulations predicted clusters of ions that change their size and shape as a function of gas loading. Saunders et al. observed similar (5–10 nm) cluster sizes (albeit on a switchable carbamate) using two-dimensional (2D) Nuclear Magnetic Resonance (NMR).[14] While spectroscopy and simulations suggest a heterogeneous solvent structure, no direct measurements have shown conclusive chemical spatial distribution to validate the suspected heterogeneity, because techniques such as IR and NMR yield bulk composition not spatial mapping of the solvent is presented.

We employed a novel in situ molecular imaging approach combining a vacuum compatible microfluidic reactor[15] and time-of-flight secondary ion mass spectrometry (ToF-SIMS) to study SWIL in this work. SIMS was used to study ionic liquids as a thin film,[16] because direct liquid analysis was deemed difficult. We developed a vacuum compatible microfluidic device, System for Analysis at the Liquid Vacuum Interface (SALVI),[15,17] and enabled liquid ToF-SIMS study of a variety of complex liquid surfaces and solid–liquid interfaces.[18–21] This work has been the

first in situ SIMS mapping of SWIL in the liquid state allowing the first spatial chemical imaging of the SWIL's solvent structure.

A schematic of the SIMS depth profiling in the microfluidic device is shown in Fig. 1b. The microfluidic channel is 200 μm wide and 300 μm deep covered by a 100 nm thick silicon nitride (SiN) membrane. During depth profiling, the Bi_3^+ primary ion beam dynamically drills holes with 2 μm in diameter on the SiN membrane and probes the liquid surface directly at the liquid–vacuum interface.[17] SIMS spectra, 2D and three-dimensional (3D) images are reconstructed from the depth profiling process (Fig. 1c–f).[19] The ionic liquid samples were also analyzed using the vacuum ultraviolet (VUV) single photon ionization mass spectrometry (SPI-MS) at the chemical dynamics beamline (9.0.2) at the Advanced Light Source (ALS). Details are described in the ESI.†

Fig. 2 depicts the representative positive ToF-SIMS spectra of SWILs loaded with different amount of CO_2. Several characteristic signals, e.g., m/z^+ 152, 153, 305, 349, 367 and 451, observed in CO_2^- loaded (i.e., 25%, 50%, 75%, 100%) samples, show much higher intensities than those in the non-CO_2 sample. The great enhancement of the protonated DBU signal (m/z^+ 153) is consistent with the ^{1}H NMR results.[1] The strong m/z^- 145 peak seen in the negative ion spectra are shown (Fig. S1, ESI†) observed after loading CO_2, indicates the formation of the $[C_6H_{13}O–CO_2]^-$ ion.
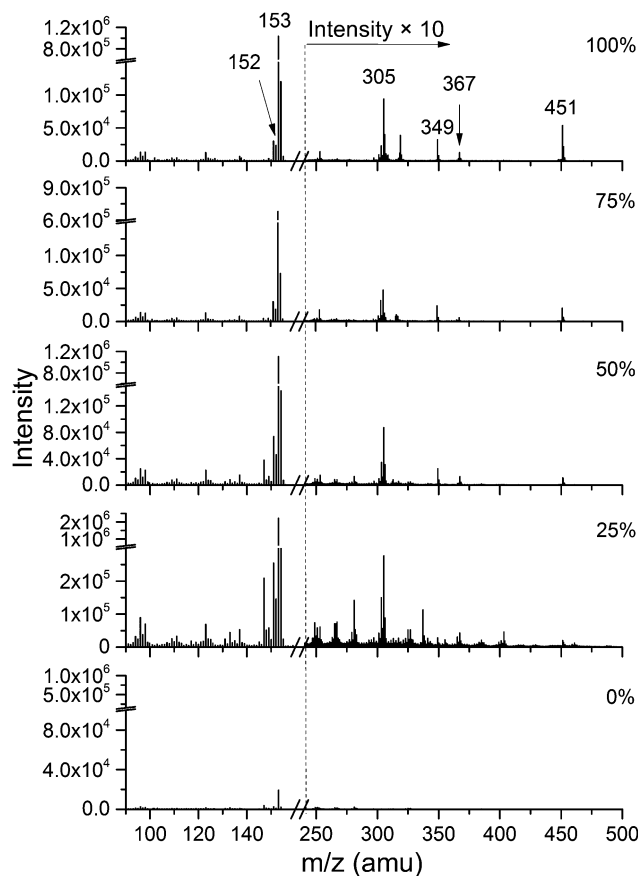

Fig. 2 Positive ToF-SIMS spectra (m/z^+ 90–500) showing comparisons of DBU and 1-hexanol loaded with 0%, 25%, 50%, 75%, and 100% CO_2, respectively.

22628 | Phys. Chem. Chem. Phys., 2017, 19, 22627–22632

This journal is © the Owner Societies 2017

This provides solid evidence of formation of ionic liquid, the structure of which is shown in Fig. 1a. Moreover, a cluster ion (m/z^+ 451) is identified, consisting of hexylcarbonate and two protonated DBU (see Table 1). Our observations not only confirm the formation of the expected carboxylated ion pair ([DBUH]$^+$ [C$_6$H$_{13}$O–CO$_2$]$^-$) but also unexpected chemical species (e.g., m/z^+ 305, m/z^+ 349),[22] indicating more complex SWIL chemistry.

Table 1 lists the identification of characteristic peaks observed in the positive and negative ion mass spectra. The formula and tentative identification for each peak are displayed. These ions are proposed based on the most likely stoichiometry of the chemical constituents in the SWIL. It should be noted that several ion clusters (composed of two or more ions), e.g., m/z^+ 367, m/z^+ 451, m/z^- 213, are observed, indicative of the ionic phase. A typical example is the m/z^+ 451 ion, which consists of a hexylcarbonate and two protonated DBU. This observation further confirms the formation of SWIL after exposure to CO$_2$. In addition, neutral molecules attached to ions (composed of an ion with one or more neutral molecules), e.g., m/z^+ 305, m/z^+ 349, and m/z^- 247, are observed, indicating there are some unreacted molecules in SWILs. The latter represents the non-ionic phase. More interestingly, some CO$_2$ molecule-attached ions, most likely due to van der Waals forces but not covalent bond, e.g., m/z^+ 349 and m/z^- 257 are observed, suggesting that some CO$_2$ molecules are physically dissolved in the SWILs. It should be noted that the neutral molecule attached ions could be observed in the more CO$_2$-loaded SWIL, indicating that not all molecules formed ions even in the so-called fully CO$_2$ loaded SWIL (100%). It is likely that there is a balance between molecules associated with CO$_2$ and other ions. Such phenomenon has not been observed using other techniques such as ex situ NMR and ATR-IR, indicating more complex SWIL chemistry.

Other DBU cluster ions (i.e., m/z^+ 305, 349, 367) are found in the CO$_2$ loaded SWILs, but relatively negligible in the CO$_2$ free non-ionic liquid. These newly identified chemical species (Table 1) indicate the ionic nature of the mixture after the CO$_2$ treatment. It is worth noting that the mass spectra obtained from the same sample is consistent, as shown in Fig. S2 (ESI†). The negative mass spectra comparison among samples and different punch-through locations in one sample are shown in Fig. S1 and S3 (ESI†). Possible negative peak identification is also listed in Table 1. Similarly, negative characteristic ionic peaks, e.g., deprotonated 1-hexanol (m/z^- 101), 1-hexanol dimer (m/z^- 247) and other CO$_2$-bonded negative ions (m/z^- 145, 213 and 257) are observed in the CO$_2$ loaded SWIL. The positive and negative SIMS mass spectral data provide complementary information of the SWILs' chemical speciation. Mass spectra of 1-hexanol and DBU individually are shown in Fig. S4 and S5 (ESI†), respectively. Representative dimers and adduct peaks shown in the SWILs are insignificant in these control samples, indicating that those peaks uniquely exist in the ionized DBU and 1-hexanol.

Interestingly, the observed solvent peaks (i.e., m/z^+ 152 and 153) and CO$_2$-bonded molecules (i.e., m/z^+ 349, 367, 451) coexist in the CO$_2$-loaded SWILs, even at 100% CO$_2$ complexation, where one would expect the only species to be the CO$_2$-bonded ion pair, represented by m/z^+ 367 and 451. This observation confirms the prediction from a recent DFT study,[13] which hypothesized that SWILs should have two phases, a polar ionic (CO$_2$-bonded) phase and a non-ionic phase. The heterogeneous liquid structure observed here differs from ILs, where the solvent remains 100% ionic regardless of the presence of CO$_2$ complexation in solution.[25–27] We rule out the possibility of the structures being liquid crystals, as X-ray diffraction patterns have not been observable in our own attempts. Neither are there any reported in the literature, to our knowledge. The structure being microemulsions is also unlikely, because emulsions are made of two immiscible and different molecules, which is inapplicable here as the liquid is essentially undergoing self-solvation. Furthermore, bi-continuous phases are not possible, as they are microemulsions that are continuous in solution, of which we see no evidence from the spatial chemical mapping.

While defined as ''switchable,'' SWILs do not simply have an ''on'' or ''off'' state; rather they have a gradient that can be tuned with CO$_2$ loading. To validate this hypothesis, various CO$_2$ loadings are studied. Both 3D imaging and spectral principal component analysis (PCA) are used. The 3D chemical mapping of the solvent structure provides details of how these dynamic structures form and insight on how they impact the properties of the fluid.

Spectral PCA is performed using selected peaks among different CO$_2$-loaded SWILs and the non-ionic liquid. Fig. 3a shows the positive spectral PC1 score versus the percentage of CO$_2$ loaded in each sample. The PC1 scores are correlated to the CO$_2$ loading percentage following a polynomial function. PC1 explains 90% of the variance. The PC1 score separates the SWIL samples loaded with 50%, 75% and 100% CO$_2$ from the non-ionic liquid (0%) and 25% CO$_2$ loaded ionic liquid. Combined with the loading results (Fig. 3b), the protonated DBU (m/z^+ 153, 305), CO$_2$-bonded species (m/z^+ 367 and 451) and CO$_2$ attached ions (m/z^+ 349) contribute to the CO$_2$-rich (i.e., 50%, 75% and 100%) ionic liquids in the positive direction of the score plot. These species are formed with increased CO$_2$ loading, indicating that the solvent changes impact on the chemical makeup depending on the degree of ionicity.

Table 1 Key peak identifications in the positive and negative ion modes

Ion mode	m/z_{obv}[a] (m/z_{cal}[b])	Formula	Possible identification[c]	Ref.
+	152 (152.13)	C$_9$H$_{16}$N$_2$$^+$	DBU$^+$	
+	153 (153.14)	C$_9$H$_{17}$N$_2$$^+$	[DBU + H]$^+$	1 and 23
+	305 (305.27)	C$_{18}$H$_{33}$N$_4$$^+$	[DBU + H]$^+$ •DBU	
+	349 (349.26)	C$_{19}$H$_{33}$N$_4$O$_2$$^+$	[DBU + H]$^+$ •DBU •CO$_2$	
+	367 (367.27)	C$_{19}$H$_{35}$N$_4$O$_3$$^+$	2[DBU + H]$^+$ [HCO$_3$]$^-$	
+	451 (451.36)	C$_{25}$H$_{47}$N$_4$O$_3$$^+$	2[DBU + H]$^+$[C$_6$H$_{13}$O CO$_2$]$^-$	
−	99 (99.08)	C$_6$H$_{11}$O$^-$	C$_6$H$_{11}$O$^-$	24
−	101 (101.10)	C$_6$H$_{13}$O$^-$	C$_6$H$_{13}$O$^-$	24
−	145 (145.09)	C$_7$H$_{13}$O$_3$$^-$	[C$_6$H$_{13}$O CO$_2$]$^-$	24
−	213 (213.12)	C$_{10}$H$_{17}$N$_2$O$_3$$^-$	[DBU + H]$^+$•[CO$_3$]$^{2-}$	
−	247 (247.19)	C$_{13}$H$_{27}$O$_4$$^-$	[C$_6$H$_{13}$O CO$_2$]$^-$•C$_6$H$_{13}$OH	
−	257 (257.11)	C$_{11}$H$_{17}$N$_2$O$_5$$^-$	[DBU + H]$^+$[CO$_3$]$^{2-}$•CO$_2$	

[a] m/z_{obv}: the unit mass m/z obtained in liquid SIMS. [b] m/z_{cal}: the calculated theoretical m/z. [c] • represents van der Waals forces, and + protonated positive ions.
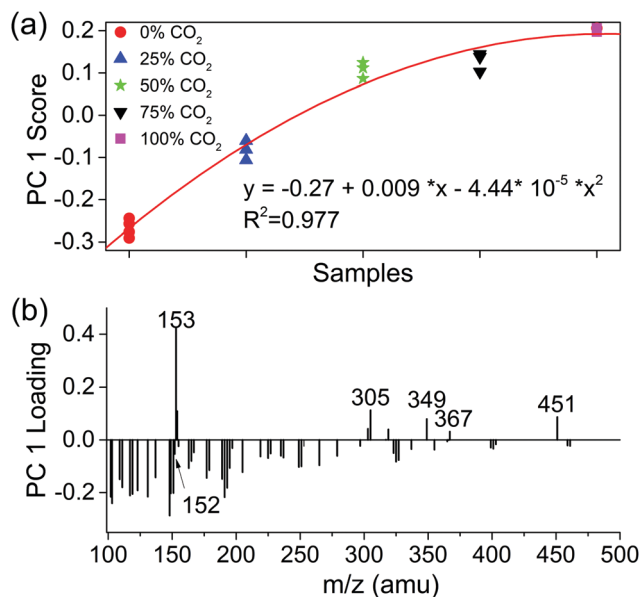
Fig. 3 PCA results of selected peaks from five samples in the positive mode. (a) The PC1 score *versus* the CO_2 loading percentage in samples. The solid red line in (a) is the least-squares fit using a polynomial function, and (b) PC1 loading plot.

The peak m/z^+ 152 is one of the key contributors to separate CO_2-lean ionic liquid (25%) and CO_2 free non-ionic liquid from highly loaded SWILs. This indicates that the DBU solvent (m/z^+ 152) is more abundant in CO_2-lean SWILs and non-ionic liquid than the CO_2 rich ones. Protonated DBU (m/z^+ 153) plays a dominant role in the distribution seen in Fig. 3a, which is in good accordance with the ionic status of the CO_2-rich SWILs, especially, with high loadings. Moreover, CO_2-rich SWILs have much larger cluster ions, indicative of the existence of ion clusters (*e.g.*, m/z^+ 305, 349, 367, 451) and the neutral molecule attached ions (*e.g.*, m/z^+ 305, 349). These larger cluster ions form with increased ionicity. The selected characteristic peaks detected in both positive and negative ion modes are presented in 2D imaging (Fig. S6, ESI†), demonstrating the relative chemical component abundance in non-ionic liquid (0%), CO_2-lean SWIL (25%) and CO_2-rich SWIL (100%), which is in good agreement with the PCA results.

The differences of chemical components among the CO_2-lean and -rich SWILs may provide insights for controlling the size and shape of clusters. This could enable applications such as controlled soft templating of nanoparticle synthesis or minimizing viscosity increases during CO_2 capture. Additionally, Fig. 3a shows the positive spectral PC1 score *versus* the percentage of CO_2 loaded in each sample. The PC1 scores are correlated to the CO_2 loading percentage following a polynomial function. This fitting result can provide information to predict the relative composition of the SWIL in relation to the CO_2 capture. For example, such correlation can be used to estimate CO_2 contents captured by the DBU and 1-hexanol SWIL. Similar observations are found in the negative spectral PCA (Fig. S7, ESI†). The spectral PCA results (Fig. S8 and S9, ESI†) using all peaks of each ion mode are also conducted, and

the results are consistent with what is shown in Fig. 3 and Fig. S7 (ESI†).

To better understand the spatial distribution of the major components in the same sample, 3D images in the positive and negative modes are reconstructed from region III in Fig. 1c for the 100% CO_2 loaded SWIL (Fig. 4). Four peaks are reconstructed in each mode. Fig. 4a shows that the ion clusters (m/z^+ 367 and 451) and the neutral molecule attached ions (m/z^+ 349) indicative of SWIL formation are not evenly distributed. In contrast, 3D image representative of the solvent components of 100% CO_2 loaded SWIL (*i.e.*, m/z^+ 152) shows a homogeneous distribution in space (Fig. 4b). This observation suggests that the SWIL solvent structure is not homogeneous as that of IL as depicted in Fig. 4b and d due to the formation of new SWIL species in Fig. 4a and c. Moreover, two liquid phases coexist. One of them more or less maintains the same feature as the non-polar solvent before CO_2 exposure, whereas the other bares the characteristics of ions and ion pairs distinctive of the SWIL as a result of CO_2 intrusion. The latter form is either *via* chemical bonding (*e.g.*, m/z^+ 367 and 451) or weak intermolecular interactions (*e.g.*, m/z^+ 349). The 3D images of these three positive ions clusters at different replicate points are shown in Fig. S12 (ESI†). Similar results (Fig. 4c and d) are found in the negative mode. The heterogeneous distribution of the negative cluster ions (m/z^- 213, 247 and 257) in Fig. 4c is in contrast to the evenly dispersed solvent species (*i.e.*, m/z^- 99) in Fig. 4d. This further confirms the heterogeneous liquid structure in SWILs. Replicate 3D images of the negative cluster ions are shown in Fig. S14 (ESI†) to provide additional evidences to support this confirmation. The SWIL was also analysed using VUV SPI-MS and the mass spectral results are complementary (Fig. S16 and Table S1, ESI†).
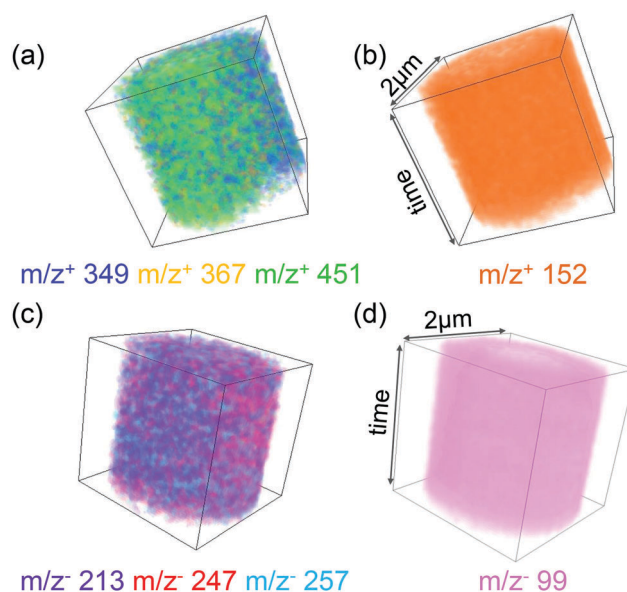

Fig. 4 3D images of selected positive and negative ion signals in the 100% CO_2 loaded sample. (a) 3D overlay image of positive ion signals (m/z^+ 349, 367 and 451), (b) 3D image of m/z^+ 152, (c) 3D overlay image of negative ion signals (m/z^- 213, 247 and 257), (d) 3D image of m/z^- 99.

22630 | *Phys. Chem. Chem. Phys.*, 2017, **19**, 22627–22632

This journal is © the Owner Societies 2017

Fig. S13 (ESI†) provides 3D images of the reference peak CH_3^+ (m/z^+ 15), DBU^+ (m/z^+ 152), and $DBUH^+$ peaks (m/z^+ 153), corresponding to the same data point at three replicate locations. The homogeneous spatial distribution of CH_3^+, DBU^+, and $DBUH^+$ peaks provides the evidence that the heterogeneity is attributed to the SWIL's intrinsic chemical nature, not a SIMS instrumental artefact, which is also supported by Fig. S15 (ESI†). In addition, the even distribution of DBU indicates that the observed heterogeneity arises from the reacted SWILs in CO_2 rich systems. More interestingly, even though these three peaks in Fig. 4a are CO_2 related, the mechanism regarding how CO_2 is bonded to DBU is different. Our measurements suggest that CO_2 can be dissolved into SWIL but not chemically bonded with the solvent, making the molecular ion m/z^+ 349 consistent with the observed lack of reactivity between DBU and CO_2.[28] In contrast, CO_2 forms the expected HCO_3^- as seen in m/z^+ 367 and hexylcarbonate and DBU ion pair in m/z^+ 451. This finding indicates that the solvent component (m/z^+ 349) and ionic components (m/z^+ 367, 451) coexist in the SWIL, even though the SWIL reaches its maximal CO_2 loading capacity of 100%. Ultimately, we conclude that this SWIL structurally cannot be considered as an IL, because non-ionic and ionic domains coexist in solution, different from an IL.

This new knowledge provides insight into the unique behaviour observed in SWILs. It is likely that the non-linear viscosity increase with CO_2 loading observed in our earlier work[29–31] is linked to the shape and size of the ionic clusters growing in solution.[13] Also, non-ionic (low polarity) regions may provide voids with high CO_2 solubility and unreacted solvent available to complex with CO_2, accounting for the higher than expected CO_2 mass transfer in and out of SWILs.[32] This may explain how a non-polar additive dissolves into solution to change the solvation free energies of the ions in solution, facilitating CO_2 release.[32] Alternatively, concentrated ionic regions could provide favourable solvation environments for catalysts for CO_2 hydrogenations[6] or precursors for nanoparticle synthesis.[8,9,12] Ultimately, discovery of this distinctive structure facilitates a deeper understanding of SWILs and how they function.

In conclusion, our findings provide the first direct observation of a dynamic and distinctive heterogeneous solvent structure of SWILs with chemical speciation previously unconceived. *In situ* chemical imaging of the air and pressure sensitive organic solvents enabled by a microfluidic reactor and imaging mass spectrometry provides spatial chemical mapping of the presence of two existing liquid phases in SWILs. Spectral analysis shows that the SWIL chemistry is more complex than existing conceptualization, with different species (*e.g.*, dimers and adducts) appearing at higher CO_2 loadings due to solvent structural changes. The ability to visualize chemical spatial distribution in 3D has led to the discovery of new chemistry and first-hand evidence that the molecular structure matches theory predictions. At least structurally, SWILs may not be ionic liquids after all; as even at 100% CO_2 loading, the liquid is comprised of two distinct phases (one more like an ionic solvent and the other a non-ionic solute) when stoichiometry would indicate otherwise. We postulate that this distinctive

molecular structure may be linked to unique behaviour observed in SWILs. Ultimately, this knowledge provides insight into SWIL behaviour and knowledge that may enhance CO_2 capture, separations, catalysis and nanoparticle synthesis, thereby making these green solvents more prominent in the chemical industry.

Acknowledgements

References

1 P. G. Jessop, D. J. Heldebrant, X. Li, C. A. Eckert and C. L. Liotta, *Nature*, 2005, **436**, 1102.

2 P. G. Jessop, S. M. Mercer and D. J. Heldebrant, *Energy Environ. Sci.*, 2012, **5**, 7240–7253.

3 D. J. Heldebrant, C. R. Yonker, P. G. Jessop and L. Phan, *Energy Environ. Sci.*, 2008, **1**, 487–493.

4 E. Privalova, M. Nurmi, M. S. Marañón, E. V. Murzina, P. Mäki-Arvela, K. Eränen, D. Y. Murzin and J. P. Mikkola, *Sep. Purif. Technol.*, 2012, **97**, 42–50.

5 S. M. Mercer and P. G. Jessop, *ChemSusChem*, 2010, **3**, 467–470.

6 M. Yadav, J. C. Linehan, A. J. Karkamkar, E. van der Eide and D. J. Heldebrant, *Inorg. Chem.*, 2014, **53**, 9849–9854.

7 P. Lozano, J. M. Bernal and A. Navarro, *Green Chem.*, 2012, **14**, 3026–3033.

8 D. Lao, R. K. Kukkadapu, L. Kovarik, B. W. Arey, D. J. Heldebrant and S. K. Nune, *Curr. Inorg. Chem.*, 2016, **6**, 92–99.

9 V. Khare, C. Ruby, S. Sonkaria and A. Taubert, *Int. J. Precis. Eng. Manuf.*, 2012, **13**, 1207–1213.

10 T. Gutel, C. C. Santini, K. Philippot, A. Padua, K. Pelzer, B. Chaudret, Y. Chauvin and J.-M. Basset, *J. Mater. Chem.*, 2009, **19**, 3624–3631.

11 A. L. Ethier, E. C. Hart, S. R. Saunders, E. J. Biddinger, A. Z. Fadhel, C. Dilek, P. Pollet, C. A. Eckert and C. L. Liotta, *Green Mater.*, 2014, **2**, 54–61.

12 S. Hardy, I. M. de Wispelaere, W. Leitner and M. A. Liauw, *Analyst*, 2013, **138**, 819–824.

13 D. C. Cantu, J. Lee, M.-S. Lee, D. J. Heldebrant, P. K. Koech, C. J. Freeman, R. Rousseau and V.-A. Glezakou, *J. Phys. Chem. Lett.*, 2016, **7**, 1646–1652.

14 T. R. Graham, R. Renslow, N. Govind and S. R. Saunders, *J. Phys. Chem. C*, 2016, **120**, 19837–19847.

15 L. Yang, X.-Y. Yu, Z. Zhu, T. Thevuthasan and J. P. Cowin, *J. Vac. Sci. Technol., A*, 2011, **29**, 061101.

16 J. Günster, O. Höfft, S. Krischok and R. Souda, *Surf. Sci.*, 2008, **602**, 3403–3407.

17 L. Yang, X.-Y. Yu, Z. Zhu, M. J. Iedema and J. P. Cowin, *Lab Chip*, 2011, **11**, 2481–2484.

18 B. Liu, X.-Y. Yu, Z. Zhu, X. Hua, L. Yang and Z. Wang, *Lab Chip*, 2014, **14**, 855–859.

19 Y. Ding, Y. Zhou, J. Yao, C. Szymanski, J. Fredrickson, L. Shi, B. Cao, Z. Zhu and X.-Y. Yu, *Anal. Chem.*, 2016, **88**, 11244–11252.

20 J. Yu, Y. Zhou, X. Hua, S. Liu, Z. Zhu and X.-Y. Yu, *Chem. Commun.*, 2016, **52**, 10952–10955.

21 X. Hua, M. J. Marshall, Y. Xiong, X. Ma, Y. Zhou, A. E. Tucker, Z. Zhu, S. Liu and X.-Y. Yu, *Biomicrofluidics*, 2015, **9**, 031101.

22 D. J. Heldebrant, P. K. Koech, J. E. Rainbolt and F. Zheng, *Energy Procedia*, 2011, **4**, 216–223.

23 J. Yao, Y. Zhou, X. Sui, D. Lao, D. Heldebrant, Z. Zhu and X.-Y. Yu, *Surf. Sci. Spectra*, 2016, **23**, 9–28.

24 Y. Zhou, J. Yao, Y. Ding, J. Yu, X. Hua, J. E. Evans, X. Yu, D. B. Lao, D. J. Heldebrant, S. K. Nune, B. Cao, M. E. Bowden, X.-Y. Yu, X.-L. Wang and Z. Zhu, *J. Am. Soc. Mass Spectrom.*, 2016, **12**, 2006–2013.

25 E. D. Bates, R. D. Mayton, I. Ntai and J. H. Davis, *J. Am. Chem. Soc.*, 2002, **124**, 926–927.

26 B. Gurkan, B. F. Goodrich, E. M. Mindrup, L. E. Ficke, M. Massel, S. Seo, T. P. Senftle, H. Wu, M. F. Glaser, J. K. Shah, E. J. Maginn, J. F. Brennecke and W. F. Schneider, *J. Phys. Chem. Lett.*, 2010, **1**, 3494–3499.

27 C. Wang, H. Luo, D.-e. Jiang, H. Li and S. Dai, *Angew. Chem., Int. Ed.*, 2010, **49**, 5978–5981.

28 D. J. Heldebrant, P. G. Jessop, C. A. Thomas, C. A. Eckert and C. L. Liotta, *J. Org. Chem.*, 2005, **70**, 5335–5338.

29 P. K. Koech, J. Zhang, I. V. Kutnyakov, L. Cosimbescu, S.-J. Lee, M. E. Bowden, T. D. Smurthwaite and D. J. Heldebrant, *RSC Adv.*, 2013, **3**, 566–572.

30 F. Zheng, D. J. Heldebrant, P. M. Mathias, P. Koech, M. Bhakta, C. J. Freeman, M. D. Bearden and A. Zwoster, *Energy Fuels*, 2016, **30**, 1192–1203.

31 D. J. Heldebrant, V.-A. Glezakou, P. K. Koech, P. Mathias, D. Cantu, R. Rousseau, D. Malhotra, M. Bhakta, M. D. Bearden, C. J. Freeman and F. Zheng, *Energy Procedia*, 2014, **63**, 8144–8152.

32 P. M. Mathias, K. Afshar, F. Zheng, M. D. Bearden, C. J. Freeman, T. Andrea, P. K. Koech, I. Kutnyakov, A. Zwoster, A. R. Smith, P. G. Jessop, O. G. Nik and D. J. Heldebrant, *Energy Environ. Sci.*, 2013, **6**, 2233–2242.